energies

MDPI

Article

# A Novel Interwell Connectivity Identification Method Based on Segmented Matching of Injection–Production Rate Fluctuations

**Hao Sun [1], Chao Yang [1,*], Zhaohui Xia [1], Yuedong Lu [1], Jianbo Liu [1], Huajun Hu [2] and Heng Yang [2]**

[1] Research Institute of Petroleum Exploration and Development, PetroChina, Beijing 100083, China
[2] China National Oil and Gas Exploration and Development Company Ltd., Beijing 100034, China
* Correspondence: yangchao2013@petrochina.com.cn

## Abstract

Accurate interwell connectivity characterization is critical for fine-grained waterflood optimization and reservoir management, often requiring integrated analysis across multiple disciplines and methods. Among these, injection–production response analysis stands as the most cost-effective and widely adopted approach. However, it remains highly subjective, heavily reliant on senior engineers' decades of accumulated experience, and prohibitively labor-intensive for large-scale oilfields with hundreds of wells. With the exponential growth of production data in modern oilfields, manual analysis has become the bottleneck restricting the timeliness of reservoir management decisions. While signal processing techniques offer a promising path to automation, general-purpose algorithms fail to incorporate fundamental reservoir fluid flow laws, resulting in insufficient accuracy for practical engineering applications. To address this gap, we propose a novel connectivity identification method that mimics expert analysis logic by focusing on large-amplitude fluctuation segments rather than full-curve matching. Using curve slope as the core metric, cosine similarity quantifies trend consistency, while Root Mean Square Error (RMSE) measures amplitude proximity. Three targeted strategies enhance accuracy: key region screening with segmented matching, outlier removal accounting for time-varying lags, and multi-index weighted fusion. Validated on synthetic and mature carbonate waterflood field cases, the method improves the identification performance over benchmark Normalized Cross-Correlation (NCC) and Capacitance-Resistance Model (CRM) methods by more than 12% in both cases. It retains the reliability of traditional response analysis while achieving full automation, and can help estimate the timing of preferential flow path formation, requiring only routine production data to provide valuable reference for timely field development decision-making.

**Keywords:** interwell connectivity identification; segmented matching; fine-grained waterflood optimization; signal processing techniques; injection–production response analysis



Academic Editor: Krzysztof Skrzypkowski

Received: 27 July 2026
Revised: 4 September 2026
Accepted: 8 September 2026
Published: 10 September 2026



## 1. Introduction

In the middle-to-late stages of waterflooding development, characterization of interwell connectivity between injection and production wells enables accurate delineation of subsurface flow paths of injected water. This, in turn, supports the design of targeted development adjustments—including water shutoff, profile control, and enhanced water injection—to ensure uniform displacement conformance and extend the economic production life of oilfields. Among conventional interwell connectivity analysis methods, tracer monitoring [1], well test analysis [2], and geochemical analysis [3] deliver high measurement accuracy, yet they disrupt normal production operations, incur high costs, and require extensive time. Numerical reservoir simulation [4] avoids production interference and lowers associated costs, but it demands a large volume of input data and involves labor-intensive workflows such as geological modeling and history matching. Injection–production response analysis is widely recognized as a robust approach and has been extensively applied even in recent years [5], but it still suffers from low analysis efficiency.

To address the limitations of the above methods, numerous scholars have proposed methods for real-time and rapid interwell connectivity characterization using dynamic production data, based on various theoretical principles. Physics-based model inversion methods [6–14] represent a key branch of interwell connectivity characterization research. However, these methods rely on inversion fitting, which introduces significant non-uniqueness and uncertainty in the results [15]. With the rapid advancement of machine learning theory in recent years, numerous scholars have applied graph neural network (GNN) models to interwell connectivity identification [16–20]. Nevertheless, machine learning-based methods generally suffer from two critical limitations: poor interpretability and weak generalization performance across different reservoir conditions.

Signal processing-based methods are developed on the fundamental principle of injection–production response analysis. In a water-flooded reservoir, injection and production wells naturally form a complete stimulus-response signal system: the injector generates an initial stimulus signal through dynamic adjustment of water injection intensity; as this signal propagates along interwell flow paths, it undergoes characteristic attenuation and time lag due to factors such as reservoir heterogeneity and the degree of flow path plugging; the fluctuations in production rate and pressure monitored at production wells are a direct manifestation of this reservoir-modified response signal. Leveraging this physical "stimulus-propagation-response" correlation, general-purpose signal processing methods can be adapted to reservoir engineering applications to decode key parameters during signal propagation, thereby enabling identification of interwell connectivity.

Tian et al. [21] proposed a modified Pearson correlation coefficient method to evaluate interwell connectivity. However, this method is built on the assumption of a linear correlation between injection and production signals, and fails to account for the lag effect of fluid flow in porous media. The Dynamic Time Warping (DTW) algorithm [20,22] quantifies the similarity between production and injection curves by calculating the optimal warping path via dynamic programming, enabling nonlinear identification of injection–production signals while accounting for time lag effects. Nevertheless, the DTW algorithm is inherently suited for single-sequence matching. Under conditions of multi-well interference, it tends to introduce irrelevant matching pairs and spurious correlations between local noise points, resulting in a deviation between the calculated similarity and the actual interwell connectivity. Wang et al. [23] evaluated multiple signal processing methods for interwell connectivity inference, and their results demonstrated that Cross-Correlation (CC) offers stronger noise immunity and outperforms DTW in scenarios with multi-well interference. Building on the CC method, Unal et al. [24] integrated wavelet transform to simultaneously capture short-term fluctuations and long-term trends in production data, making the method adaptable to non-stationary signal datasets.

However, due to the unique characteristics of reservoir systems, direct application of general-purpose signal processing algorithms to reservoir engineering often yields large calculation errors. Specifically, the time lag of injected water signal propagation in reservoirs does not vary randomly as assumed by the DTW algorithm, nor does it remain constant as postulated by the CC method. Instead, its variation conforms to a clear, physically driven rule set by the dynamic changes in reservoir flow capacity during water injection. In most cases, long-term scouring by injected water forms thief zones or induces dynamic fractures, both of which significantly increase reservoir permeability. Consequently, injected water breaks through along preferential flow paths, leading to a gradual reduction in time lag with continuous water injection. In a small subset of field cases, the time lag may also increase, which is primarily attributed to formation damage induced by poor injection water quality [25–29]. Critically, existing signal processing methods have not yet accounted for this time-varying lag behavior.

In summary, among existing interwell connectivity analysis methods, physics-based inversion and machine learning-based methods are limited by high uncertainty and insufficient reliability. By comparison, signal processing-based methods have clear physical meaning, strong interpretability, and controllable uncertainty, demonstrating significant potential for field applications. Nevertheless, two critical research gaps remain in current signal processing workflows:

1. They fail to account for the well-defined intrinsic time-varying behavior of signal lag in water-flooded reservoirs.
2. They rely on similarity matching based on the overall amplitude of the target curves, which only supports coarse-grained holistic matching and cannot accurately capture the intrinsic response characteristics of injection–production signals. Both limitations directly restrict the accuracy of interwell connectivity identification results.

This study first introduces the fundamental principle of the proposed interwell connectivity identification method. Subsequently, a synthetic reservoir model with five injectors and four producers is constructed to validate the proposed method against streamline simulation results. The method is then applied to a real oilfield case, with its effectiveness verified through comprehensive integration of production performance curve analysis, field monitoring data, and reservoir geological characteristics. The results demonstrate that the proposed method yields strong agreement with both streamline simulation outputs and the established understanding of interwell connectivity in the actual oilfield.

## 2. Methods

### *2.1. Quantitative Metrics for Similarity Characterization*

In this study, each injection–production pair is treated as a complete stimulus-response signal system, where the similarity of rate fluctuations between the production and injection wells is considered to reflect the degree of interwell connectivity. Specifically, under ideal conditions, an injection–production pair with strong interwell connectivity exhibits the following characteristics: a significant increase in injection rate is followed by a substantial rise in the liquid production rate of the producer, and a significant decrease in injection rate is accompanied by a corresponding decline in liquid production rate. Therefore, to accurately characterize interwell connectivity, the similarity calculation focuses on the similarity of the slope of the two curves, rather than the similarity of the overall curve amplitude.

Prior to similarity calculation, a data preprocessing step is performed on the raw injection and production rate series. The curves are first normalized to the range [0, 1] to eliminate the influence of different production scales, and then smoothed using a moving average filter with a window size of 3 months. This smoothing is necessary because the slope (computed as the first-order difference) is highly sensitive to high-frequency noise. For monthly sampled data, a 3-month window provides a reasonable balance between noise suppression and preservation of meaningful injection–production responses. For datasets with different sampling frequencies, the window size should be adjusted proportionally to the expected duration of significant fluctuations.

Cosine similarity is defined as the cosine of the angle between two vectors $A$ and $B$, which quantifies the similarity in the direction of the two vectors independent of their magnitude. The calculation formula is as follows:

$$\cos\theta = \frac{A \cdot B}{\|A\|\|B\|}. \tag{1}$$

The calculation result of cosine similarity falls within the interval [−1, 1]. When cosine similarity is used to calculate the similarity of the slope of two curves, a result closer to 1 indicates a higher consistency in the fluctuation trend between the injection and production wells.

Root Mean Square Error (RMSE) is adopted to measure the deviation between two equal-length paired data sequences, specifically the slope sequences of the injection and production curves in this study. The calculation formula is as follows:

$$\mathrm{RMSE} = \sqrt{\frac{\sum_{i=1}^{n}\left(y_{inj,i} - y_{pro,i}\right)^2}{n}}. \tag{2}$$

where $y_{inj,i}$ is the i-th slope data point of the injection curve, $y_{pro,i}$ is the i-th slope data point of the production curve, and n is the total number of paired data points.

The calculation result of RMSE falls within the interval [0, +∞), with a smaller value indicating a smaller deviation between the two curves. When RMSE is used to quantify the difference in the slope of two curves, a smaller RMSE under synchronous fluctuation indicates that the rise and fall amplitudes of the two curves are highly consistent.

Under the condition of multi-well interference, the consistency of fluctuation direction between the two curves is the primary focus, and a closer fluctuation amplitude is preferred under the premise of consistent fluctuation direction. Accordingly, a comprehensive metric is established to reflect the consistency of the injection–production response, with the formula as follows:

$$s = \alpha * cos\,\theta + (1-\alpha) * e^{-\mathrm{RMSE}}. \tag{3}$$

where $e^{-\mathrm{RMSE}}$ is introduced as an inverse mapping of RMSE to facilitate quantitative characterization. The calculation result of $e^{-\mathrm{RMSE}}$ falls within the interval (0, 1], with a value closer to 1 indicating higher similarity between the two curves. It should be noted that both the slope values and the RMSE are dimensionless, because the raw rate curves are normalized to the range [0, 1] prior to slope calculation. This normalization ensures that the exponential mapping $e^{-\mathrm{RMSE}}$ in Equation (3) is scale-independent and not affected by the original magnitudes of injection or production rates.

The weighting coefficient $\alpha$ controls the relative contribution of directional consistency and amplitude proximity. Based on the physical principle described above, $\alpha$ should be larger than 0.5. In this study, a sensitivity analysis with $\alpha$ varying from 0.6 to 0.8 showed that the final connectivity classification remained stable and accurate across this range for both the synthetic and field cases. Therefore, $\alpha$ = 0.7 is selected as a representative value within this stable interval. For applications to other reservoirs, the value of $\alpha$ may be adjusted within 0.6–0.8 according to the specific data characteristics, and a similar sensitivity analysis is recommended to verify the robustness of the results.

### *2.2. Target Matching Region Identification*

In conventional methods, similarity matching is performed on the entire injection and liquid production curves to quantify interwell connectivity and time lag. The workflow is as follows: the entire production curve is shifted forward by different time intervals $\Delta t$, and the similarity between the injection curve and the shifted production curve is calculated.

After multiple shifts and calculations, the time interval $\Delta t_n$ corresponding to the maximum similarity is taken as the time lag, and the corresponding maximum similarity is used as the basis for interwell connectivity discrimination of the injection–production pair. As shown in Figure 1, when the production curve is shifted by $\Delta t_2$ and achieves the highest similarity with the injection curve, $\Delta t_2$ is determined as the time lag between the injection–production pair, meaning the injection signal propagates to the producer after a duration of $\Delta t_2$.

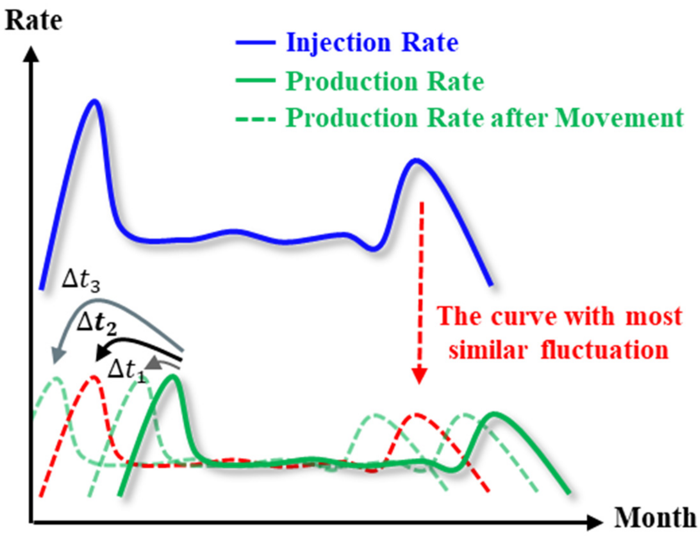


**Figure 1.** Schematic of interwell connectivity identification via full-curve holistic matching.

However, this holistic full-curve matching approach is overly idealized. In practice, the time lag of signal propagation is not constant, and production is often subject to combined multi-well interference. It is therefore difficult to determine an appropriate fixed time lag that enables a one-to-one match between the full-segment fluctuation of the production rate and the injection rate fluctuation, leading to inaccurate characterization of the interwell correspondence.

To address these limitations, this study focuses the matching target on regions with significant fluctuations in the injection curve and identifies the corresponding similar fluctuation segments in the production curve. This improvement offers two key advantages:

1. Shifting from full-curve holistic matching to target region matching enables better adaptation to complex fluctuation propagation scenarios such as time-varying time lag.
2. Selecting regions with significant fluctuations as the matching target reduces noise interference during the matching process and improves matching accuracy. This approach is underpinned by the fundamental physical principle that an injection signal with a significant rise or fall propagating along a well-connected zone will inevitably generate a distinct fluctuation response at the producer, which cannot be completely offset by other injection signals even under multi-well interference.

The implementation workflow of this improvement is as follows: first, peaks and troughs corresponding to significant fluctuations in the injection and production curves are located, respectively, using the peak detection algorithm from the open-source SciPy library [30]. On this basis, an intelligent extension strategy is proposed in this study to form target regions while avoiding null values. The principle of the peak detection algorithm is as follows: first, traverse each point in the curve to identify all potential peaks; second, calculate the prominence of each peak relative to the adjacent region; finally, set a screening threshold to retain peaks with high prominence, with only the most prominent peak retained within a specified adjacent distance. For trough detection, the peak detection algorithm is reapplied to the inverted curve to locate the positions of troughs with significant fluctuations.

Specifically, the curves are normalized to [0, 1] before peak detection. The find_peaks function from SciPy 1.16.3 is applied with two parameters: distance, the minimum interval between adjacent peaks (in data points), and prominence, the minimum relative amplitude for a peak to be considered significant. For the monthly data used in this study, distance = 6 is adopted to avoid capturing short-term noise. A two-stage detection strategy is used for prominence: it is first set to 0.2 to detect major fluctuations; if fewer than three peaks are identified, the prominence is relaxed to 0.1 and detection is repeated. These settings are illustrative; for other sampling intervals, distance should be adjusted proportionally to the expected minimum duration between meaningful events, and prominence tuned according to the typical signal-to-noise ratio.

Since the peak detection algorithm only locates the index of the center point of the peak/trough, it is necessary to extend to both sides to form a complete target region. It is worth noting that an excessively long extension range will cause the target region to include too many irrelevant curve features and interfere with the matching effect, while an excessively short extension range will extract only a small part of the fluctuation features and increase the matching error. Therefore, an intelligent extension strategy is set to form the target region with the peak/trough as the center point, as shown in Figure 2. The rules for intelligent extension are as follows:

1. Set the extension limit for both left and right sides (e.g., a limit of 3–9 months means the minimum and maximum extension distance for both sides is 3 months and 9 months, respectively). In the intelligent extension, the endpoint is normally the nearest trough or peak; however, abnormal values may cause premature truncation. The 3-month minimum helps ensure that a complete fluctuation cycle is captured, while the 9-month maximum prevents the region from including excessive unrelated segments and thus avoids the limitations of full-curve matching. These values are illustrative and can be adjusted according to the characteristics of the target dataset.
2. Identify the extension endpoint within the limit: for a peak center point, the nearest trough positions on the left and right sides are taken as the extension endpoints, and vice versa for a trough center point.
3. If extension stops on one side due to null values and the extension distance is less than 3 months, additional extension is performed on the other side within the set limit.

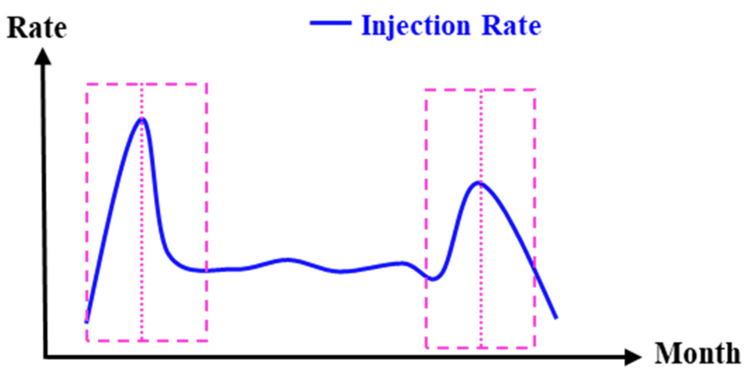


**Figure 2.** Identification of key target regions with significant fluctuations.

### *2.3. Segmented Matching Workflow*

Since a single curve may contain multiple target matching regions, this study adopts a workflow of segmented matching followed by weighted fusion. The segmented matching workflow is shown in Figure 3:

1. Locate regions with significant fluctuations in the injection curve to extract multiple target segments;
2. For each target segment, calculate and identify the fluctuation segment on the production curve with the same length and the highest similarity;
3. Count and retain the characteristic values of the corresponding most similar production segments in chronological order of the target regions, including time lag $\Delta t$, similarity $s$, amplitude weight $\lambda$, and the position index of the production segment center point $x_{pro}$.

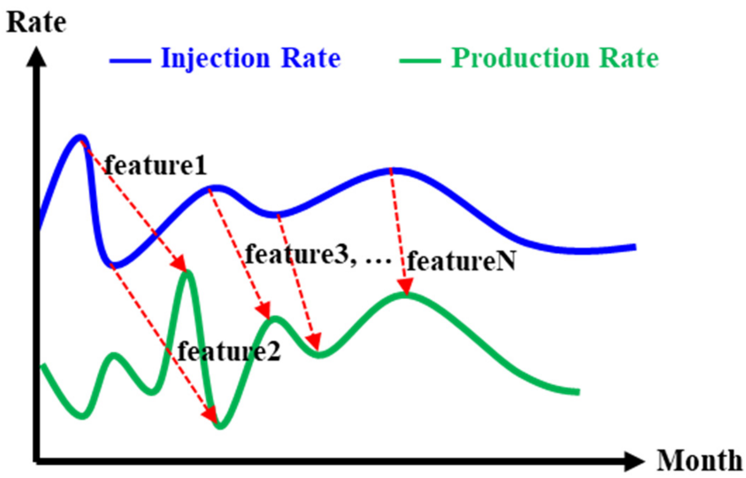


**Figure 3.** Schematic of segmented matching.

A physical constraint is enforced during matching: since the propagation of the injection signal in the subsurface requires time, matching can only be performed starting from at least one time step after the time point corresponding to the center of the injection target region. In addition, an unreasonably long propagation time is excluded, and matching is limited within a specified time span.

The calculation formula for the amplitude weight $\lambda$ is as follows:

$$\lambda = \left|max\left(y_{inj}\right) - min\left(y_{inj}\right)\right| \cdot \left|max\left(y_{pro}\right) - min\left(y_{pro}\right)\right|. \tag{4}$$

where $y_{inj}$ represents the curve value in the injection target segment, and $y_{pro}$ represents the curve value in the matched production segment.

## 2.4. Outlier Filtering Strategies

Although segmented matching can theoretically achieve more accurate one-to-one matching of injection and production fluctuations, the most similar fluctuation identified by matching may not be the most physically reasonable one due to multi-well superposition effects or accidental factors. In addition to focusing on significant fluctuation regions and weighted fusion, this study adopts credibility filtering and outlier filtering strategies to mitigate the impact of such incorrect matching.

### 2.4.1. Credibility Filtering

The credibility filtering strategy is formulated based on the magnitude of the similarity s and amplitude weight $\lambda$ for each matched correspondence. A higher fluctuation amplitude of the injection segment, a higher fluctuation amplitude of the matched production segment, and a higher similarity between the two indicate a higher credibility of the matching result. In practice, although each injection fluctuation segment will match to the production segment with the relatively highest similarity, the absolute value of this maximum similarity may be very low. Accordingly, the credibility screening rules are established as follows:

1. If multiple injection fluctuation segments are matched to the same production segment, only the correspondence with the highest product of amplitude weight and similarity $\lambda \cdot s$ is retained.
2. The interquartile range method is used to remove all correspondences with $\lambda \cdot s$ lower than the first quartile (the 25th percentile of all data sorted in ascending order).
3. Only correspondences with similarity s greater than 0.5 are retained. Since s ranges from 0 to 1, this empirical threshold excludes correspondences whose similarity is less than half of the theoretical maximum, thereby reducing the influence of spurious matches. The value of 0.5 is not fixed and can be adjusted depending on data quality and the desired confidence level for a given application.

### 2.4.2. Physical Law-Based Outlier Filtering

The outlier filtering strategy is formulated based on the variation law of time lag $\Delta t$ for each correspondence, to remove correspondences that are obviously inconsistent with physical laws. Due to long-term scouring by injected water, particles in the reservoir skeleton are continuously carried away, leading to a gradual decrease in the time lag of the injection signal over time. The outlier removal rules considering this physical law are as follows:

1. Head and tail anomaly: the first data point with an excessively small value or the last data point with an excessively large value is removed;
2. Single-point anomaly: a data point is removed if the values before and after it are close, but the point itself differs significantly from the adjacent values (as shown in Figure 4);
3. Continuous anomaly: continuous clusters of excessively large or small values are removed if the values before and after the cluster are close.

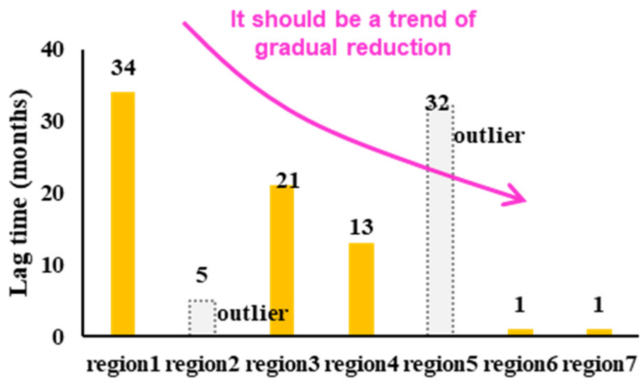


**Figure 4.** Schematic of outlier filtering.

In the example shown in Figure 4, 7 key fluctuation regions in the injection curve are matched to the production curve, corresponding to 7 time lag values. Among them, the time lags of region 1 (34 months) and region 3 (21 months) are relatively large, while the time lag of region 2 (5 months) is abnormally small, which does not conform to the gradual decreasing trend. Therefore, the correspondence for region 2 is removed according to the rules. Similarly, the time lag of region 5 (32 months) is abnormally large compared with that of region 4 (13 months) and region 6 (1 month), so the correspondence at region 5 is also removed.

*2.5. Identification of Preferential Flow Path Formation Timing*

Long-term scouring by injected water may lead to the formation of water-flooding preferential flow paths between injection and production wells, which will cause a significant reduction in the time lag of the injection signal after formation. Based on this principle, the turning point where the downward trend of time lag increases sharply is calculated to provide a rough estimate of the formation timing of preferential flow paths. As shown in Figure 4, after outlier removal, the time lag decreases significantly from region 4 (13 months) to region 6 (1 month) and region 7 (1 month), indicating that preferential flow paths may have been formed at the time corresponding to region 6.

Identifying existing preferential flow paths or providing early warning of impending preferential flow path formation can help reservoir engineers conduct further analysis and formulate targeted adjustment measures, thereby reducing invalid water circulation and improving water flooding sweep efficiency.

*2.6. Weighted Fusion and Connectivity Classification*

The similarity and time lag obtained from segmented matching are characteristics corresponding to multiple target regions on the well curves. To quantify the overall interwell connectivity and comprehensive signal propagation time lag of the injection–production pair, the similarity values and time lag values from multiple matched segments are separately fused via weighted averaging into two independent comprehensive metrics, while the core information from critical segments is maximally retained. The weighting principles are as follows:

1. A higher weight is assigned to segments with larger fluctuation amplitude;
2. A higher weight is assigned to segments with higher matching similarity;
3. A higher weight is assigned to injection–production pairs with more valid matched segments (more remaining matched segments after multi-layer screening indicate potentially stronger interwell connectivity between the injection–production pair);
4. A higher weight is assigned to correspondence with an incrementally increasing center point index of the production segment $x_{pro}$ (non-crossed connecting lines of injection–production matched segments indicate more reasonable matching results).

Figure 5 shows the complete workflow for calculating the similarity and time lag between an injector and a producer. When there are multiple producers around an injector, the similarity between the injector and each surrounding producer is calculated sequentially and sorted to reflect the relative strength of interwell connectivity between the injector and the surrounding producers. Although the theoretical range of the similarity $s$ is $-1$ to 1, the region is shifted left and right during matching to find the maximum similarity, so the actual obtained s falls within the interval (0, 1], and the weighted average result also falls within (0, 1]. That is, the calculation results of all interwell connectivity are between 0 and 1, so the relative strength of global interwell connectivity can be determined by the magnitude of the similarity. In this study, interwell connectivity is divided into four grades: no connectivity ($0 < s \leq 0.25$), poor connectivity ($0.25 < s \leq 0.5$), moderate connectivity ($0.5 < s \leq 0.75$), and strong connectivity ($0.75 < s \leq 1$).

The thresholds 0.25, 0.5, and 0.75 are used to classify the continuous similarity values into four connectivity grades. These values are empirical and were selected to provide a meaningful interpretation of the similarity metric for the target reservoir, consistent with the available field connectivity knowledge. They are not universal constants and may be adjusted for other reservoirs based on the distribution of computed similarities and the specific requirements of the application.

https://doi.org/10.3390/en19184285

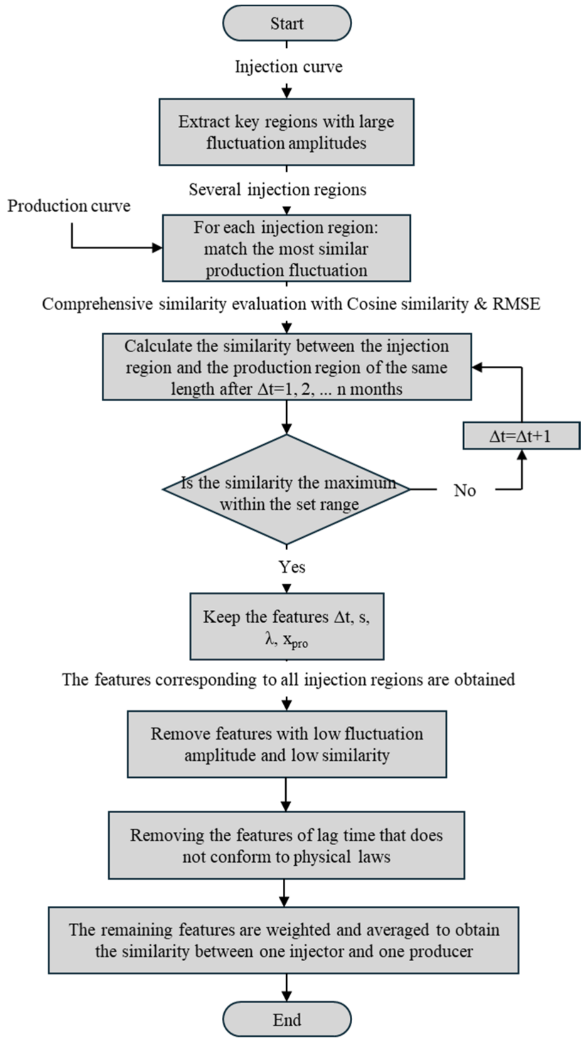


**Figure 5.** Flowchart of matching process for single injection–production pair.

## 3. Results

The performance of the proposed method was validated via application to one synthetic case and one real field case.

### 3.1. Case 1: Synthetic Case

A synthetic heterogeneous reservoir model was constructed to validate the proposed method, as shown in Figure 6. The model contains 4 producers and 5 injectors with a well spacing of 900 m, and the matrix permeability is 50 mD. High-permeability streaks are developed between injection and production wells: the permeability between I1 and P1 is 2000 mD, and the permeability between I2 and P1, I4 and P2, as well as I5 and P3 is 800 mD.

The synthetic reservoir was put into production in February 1999, with a total production period of 35 years. The injection mode of injectors was controlled by flow rate (as shown in Figure 7), and producers were operated by bottomhole pressure (BHP).

The time-series data of liquid production rate from producers and water injection rate from injectors were collected and preprocessed, and the proposed method was applied for interwell connectivity analysis. The identification results of the proposed method are illustrated by taking well I1 as an example, as shown in Figure 8.

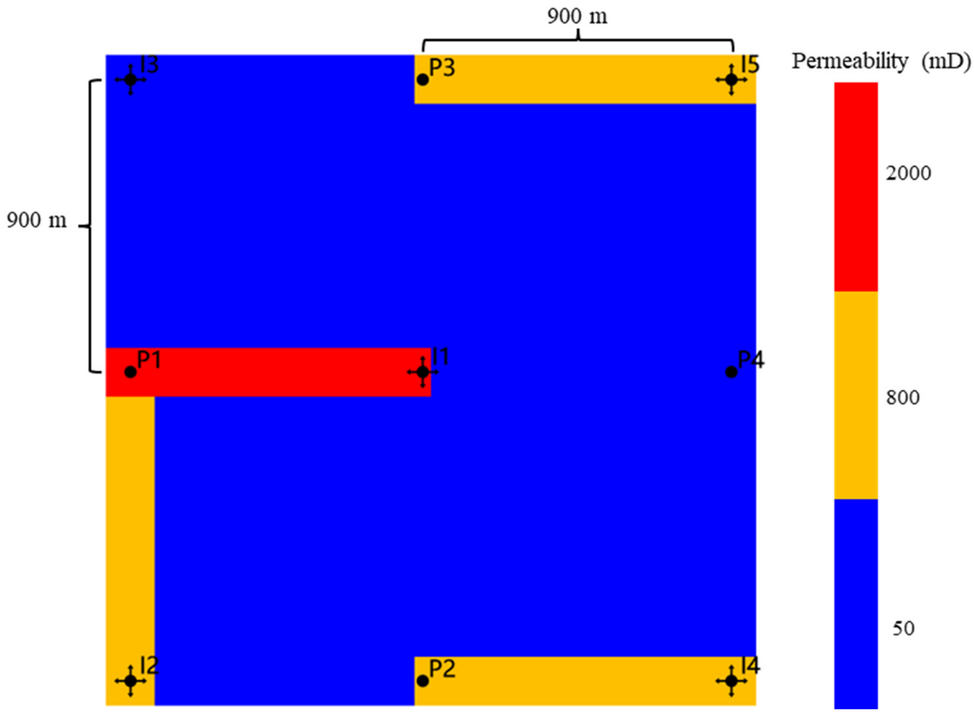


**Figure 6.** Planar permeability distribution of the 5-injector 4-producer conceptual model.

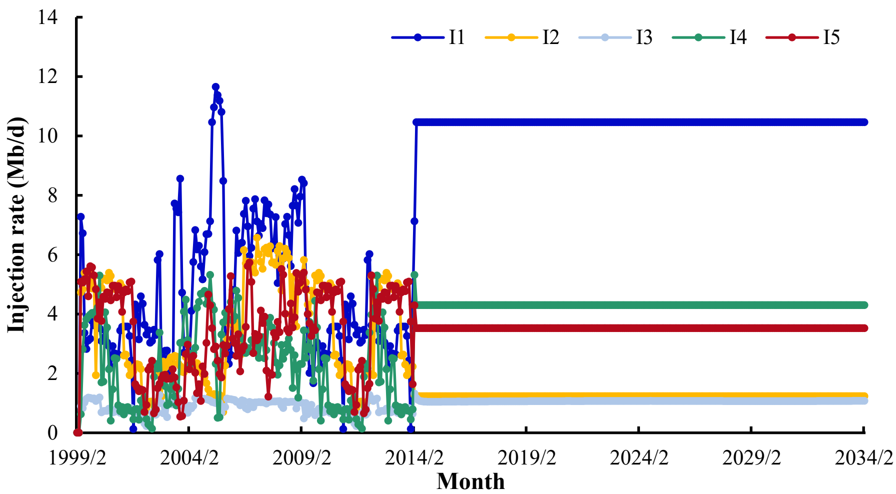


**Figure 7.** Injection rate profiles of five injectors in the synthetic case.

Figure 8 shows that the proposed method identified the strongest interwell connectivity between I1 and P1, with a comprehensive similarity of 0.9, which is significantly higher than that of other injection–production pairs. This is consistent with the geological setting of the synthetic model, where only a high-permeability streak exists along the direction from I1 to P1 around well I1. The colored regions in Figure 8 mark the basis for the identification of the proposed method: three significant fluctuation events of well I1 all generated highly similar fluctuation responses at well P1. From the green area marked around 2010, it can be seen that the similarity identified by the proposed method is not the similarity of curve amplitude (as the amplitudes of the two curves show little proximity across the entire target segment). The method accurately captures the synchronization of fluctuations and the similarity of rise and fall amplitudes in the key regions, thus reasonably reflecting the strength of interwell connectivity.

https://doi.org/10.3390/en19184285

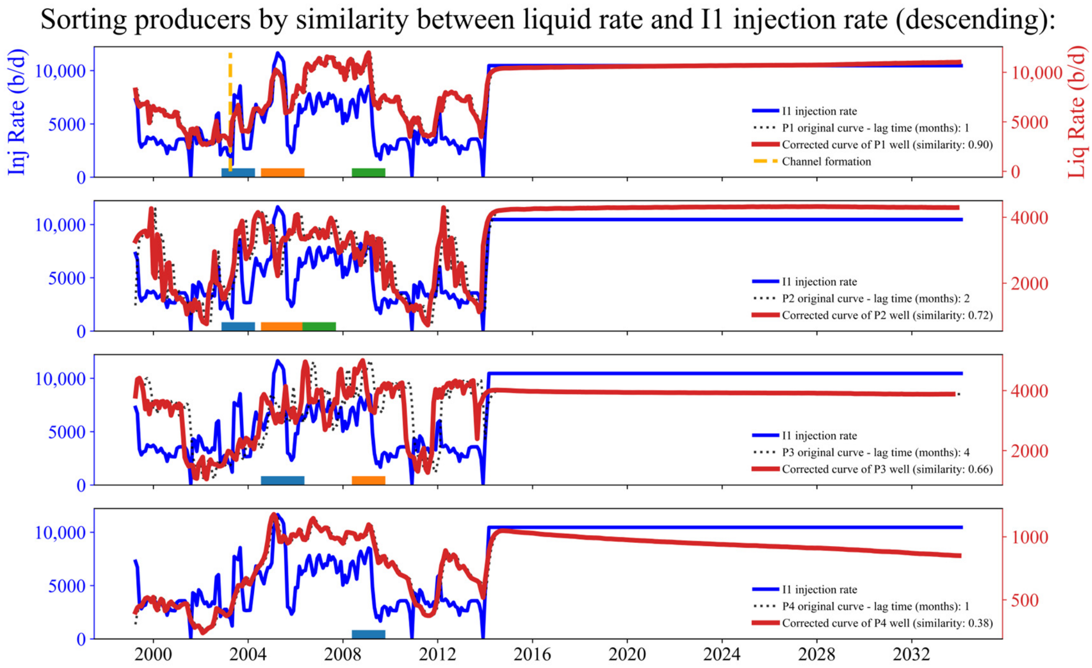


**Figure 8.** Connectivity analysis for well I1 by the proposed method in synthetic case. Note: yellow line: advantageous channels formed from this point; red line: original liquid production curve shifted forward by lag time; colored regions on the x-axis: fluctuation zones analyzed by this method.

In contrast, the similarity of curve amplitude does not interfere with the connectivity results. After 2014, the long-segment curve morphology of the other three producers is very close to that of well I1, but the calculated interwell connectivity remains low because the proposed method only focuses on the key fluctuation regions. The number of identified similar segments also affects the final connectivity results: well I1 has fewer similar segments with P3 and P4, and the similarity of fluctuation responses is lower, so the final comprehensive similarity is much lower than that with P1.

### *3.2. Case 2: Real Field Case*

The real field case is selected from Reservoir M in the Middle East, which is a porous carbonate reservoir with developed high-permeability streaks, a lack of stable continuous interlayers between formations, and extremely strong heterogeneity. The reservoir was developed by depletion drive starting from 1999, and large-scale water flooding was implemented in 2014 with an inverted nine-spot well pattern.

A typical well group was selected to validate the proposed method, which contains eight producers with an average daily oil production of 3000 bbl/d. To compensate for the severe formation pressure depletion in the early development stage, the injector adopted an extremely high daily water injection rate, with an average of 12,000 bbl/d and a maximum of nearly 30,000 bbl/d. After injection well I1 was shut in May 2023, both wells P1 and P6 showed a significant decrease in water cut and an increase in oil production. When well I1 resumed injection in January 2025, wells P1 and P6 subsequently showed a rapid rise in water cut and a decline in oil production, while no obvious response was observed in other wells. The analysis results of Production Logging Tool (PLT) monitoring data show that the main fluid-producing intervals of P1 and P6 are completely consistent with the main water intake intervals of I1. From the geological model, the locations of wells P1 and P6 also meet the development conditions of high-permeability streaks. Based on the comprehensive understanding of multiple data sources, it is confirmed that well I1 has strong interwell connectivity with P1 and P6, and weak connectivity with other wells.

The proposed method was applied to conduct interwell connectivity analysis for this well group, with the input data truncated to May 2023. The purpose of this setting is to verify whether the proposed method can identify interwell connectivity consistent with the above comprehensive analysis results before the injection well was shut in. As shown in Figure 9, the comprehensive similarity of P1 and P6 is greater than 0.75, which is consistent with the understanding of strong interwell connectivity between I1-P1 and I1-P6 obtained from the comprehensive multi-data analysis. The calculated connectivity of wells P2 and P4 is 0, so they are not shown in the figure.

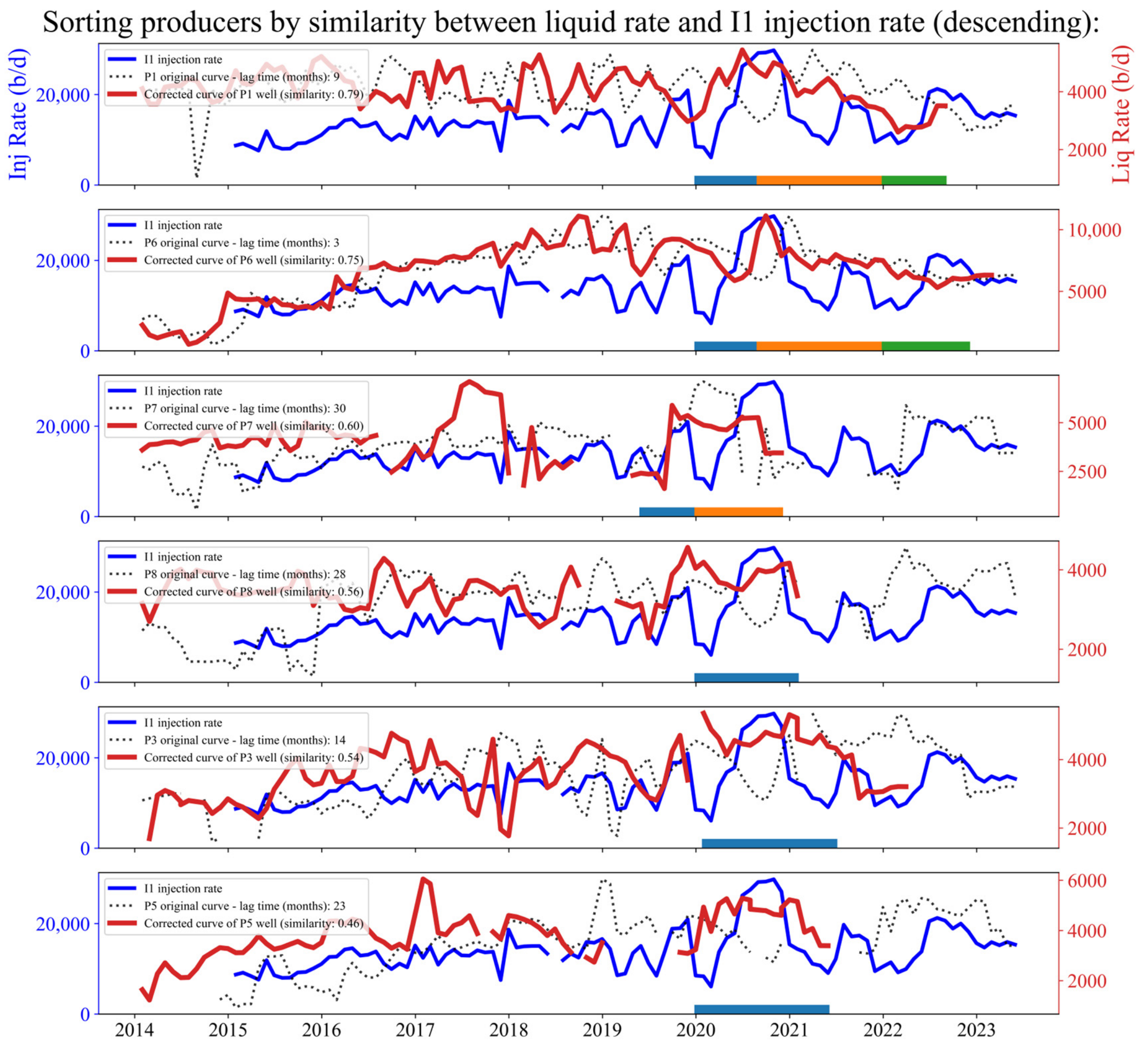


**Figure 9.** Connectivity analysis for well I1 by the proposed method in real field case. Note. Yellow line: advantageous channels formed from this point; red line: original liquid production curve shifted forward by lag time; colored regions on the x-axis: fluctuation zones analyzed by this method.

In real field scenarios, production and injection wells inevitably experience frequent shut-in and shut-down events, which pose great challenges to conventional full-curve similarity comparison methods. Most existing methods cannot accommodate null values in the input data; however, filling missing values with zeros will introduce significant interference to similarity calculation and may incorrectly identify injection–production pairs with long zero-value segments as strongly correlated. As shown in Figure 9, the proposed method in this study has good adaptability to well data containing null values:

the selected key regions automatically avoid null value positions, which does not interfere with the calculation of interwell connectivity and time lag.

### *3.3. Comparative Analyses*

The performance of the proposed method was validated against two widely used benchmark methods via application to both the synthetic and real field cases. The benchmark methods selected for comparison are the Cross-Correlation (CC) method [31] and the Capacitance-Resistance Model (CRM) [7].

Cross-Correlation (CC) is a statistical method for quantifying the similarity between two signals or time series. Its core principle is to calculate the similarity of two signals at different time lags to determine their relative time delay and correlation. Given that the injection and production rate data may have different scales, the Normalized Cross-Correlation (NCC) was adopted in this study for comparison. In addition, the time lag calculated by NCC was constrained to positive values to comply with physical laws, i.e., the correlated fluctuation of the production well cannot occur prior to the corresponding fluctuation of the injection well.

The Capacitance-Resistance Model (CRM) is currently the mainstream method for quantitative evaluation of interwell connectivity in reservoirs. Based on the material balance principle, CRM treats the interwell unit as a series system of "fluid storage capacity and seepage resistance", and inverts the interwell connectivity coefficient via history matching of injection and production data. In this study, the CRM was configured using only injection and liquid production rate data. No bottomhole pressure data were used.

For the CRM and NCC methods, missing values were filled with zeros. In the field data, monthly production records are complete, and missing values correspond only to shut-in periods with zero actual flow; thus, zero-filling is accurate. In contrast, the proposed method requires no filling, as the segmented matching automatically identifies key regions and avoids missing or zero intervals, making it suitable for fields with frequent shut-ins.

#### 3.3.1. Synthetic Case Comparison

In the synthetic case, the flow rate allocation of each injector was obtained via streamline simulation, as shown in Figure 10a. The calculation results of the proposed method, NCC and CRM (Figure 10b–d) were compared against the streamline simulation results to verify the performance of the proposed method. The results of the proposed method and NCC both fall within the interval (0, 1], and the CRM results were normalized to the same interval for consistent comparison.

As can be observed from Figure 10, the interwell connectivity derived from NCC shows relatively poor agreement with the streamline simulation results; the direction of maximum connectivity calculated by CRM is generally consistent with the direction of dense streamlines, but there is one misclassification—CRM identified strong connectivity between I3 and P1, while no actual high-permeability connection exists between this injection–production pair; and the connectivity results of the proposed method show the highest agreement with the streamline simulation outputs.

To quantitatively evaluate the consistency between the calculated connectivity and the actual results, the matching performance was simplified to a binary classification problem and evaluated using the F1-score. The F1-score is the weighted harmonic mean of precision and recall, ranging from 0 (worst performance) to 1 (perfect performance). The calculation formula is as follows:

$$F_1 = 2\frac{precision \cdot recall}{precision + recall}, \tag{5}$$

where precision represents the proportion of predicted preferential flow directions that are actual preferential flow directions, calculated by Equation (6); recall represents the

https://doi.org/10.3390/en19184285

proportion of correctly identified actual preferential flow directions out of all real preferential flow directions, calculated by Equation (7).

$$precision = \frac{TP}{TP + FP}, \quad (6)$$

$$recall = \frac{TP}{TP + FN}. \quad (7)$$

In the above equations, TP (True Positive): correctly predicted positive cases; TN (True Negative): correctly predicted negative cases; FP (False Positive): incorrectly predicted positive cases; and FN (False Negative): incorrectly predicted negative cases.

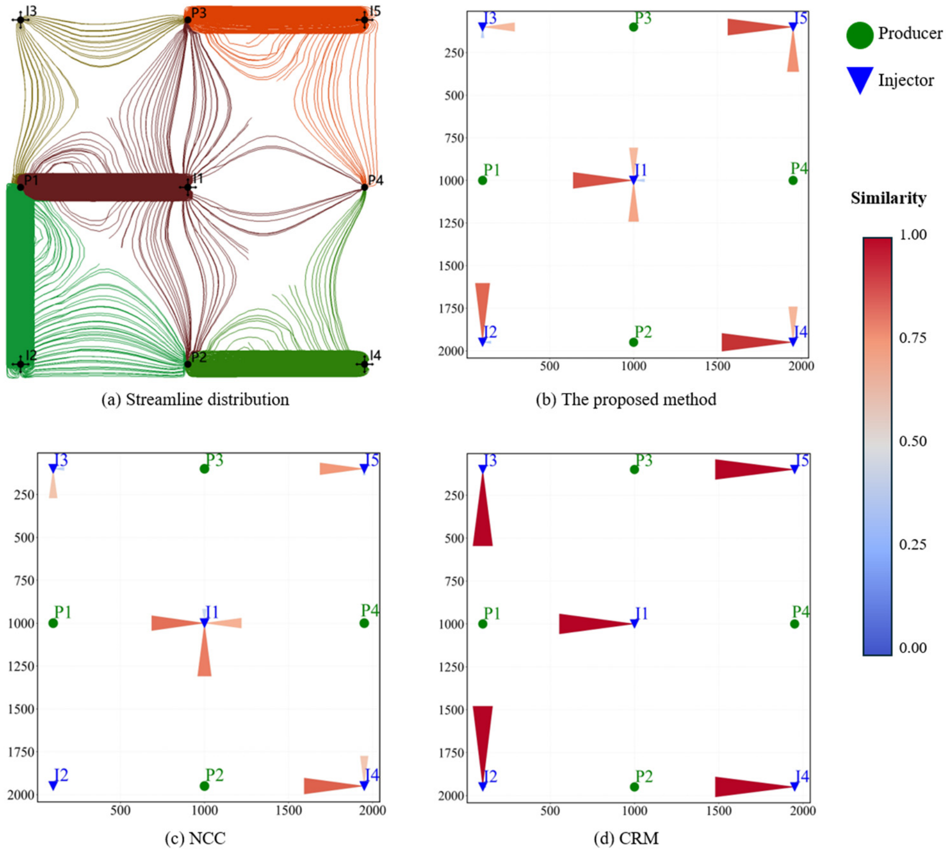


**Figure 10.** Comparison between streamline simulation and various connectivity calculation methods. Note: (**a**) streamline distribution of injectors (different colors for different injectors); (**b**–**d**) connectivity distribution centered on the injector using different methods. Stronger connectivity is shown in red with longer and wider strips; weaker connectivity appears in blue with shorter and narrower strips.

The connectivity results from each method were taken as the predicted values and classified into preferential flow directions (positive cases, similarity > 0.75) and non-preferential directions (negative cases, similarity $\leq$ 0.75). The streamline simulation results were taken as the ground truth, with dense streamline regions defined as preferential flow directions (positive cases) and the rest as non-preferential directions (negative cases). The performance of each method, calculated via Equations (5)–(7), is summarized in Table 1.

Table 1 shows that the proposed method achieves an F1-score of 1, indicating that its calculated connectivity for both preferential and non-preferential flow directions is perfectly consistent with the ground truth. CRM also delivers good performance with an F1-score of 0.89, with only one misclassification in a non-preferential direction. NCC shows relatively poor performance with an F1-score of 0.75, with one misclassification in each of the preferential and non-preferential directions.

**Table 1.** Matching degree between calculated connectivity and actual results.

| Injector–Producer Pair | Actual | The Proposed Method | NCC | CRM |
|---|---|---|---|---|
| I1-P1 | Positive | Positive | Positive | Positive |
| I1-P2 | Negative | Negative | Positive | Negative |
| I1-P3 | Negative | Negative | Negative | Negative |
| I1-P4 | Negative | Negative | Negative | Negative |
| I2-P1 | Positive | Positive | Negative | Positive |
| I2-P2 | Negative | Negative | Negative | Negative |
| I3-P1 | Negative | Negative | Negative | Positive |
| I3-P3 | Negative | Negative | Negative | Negative |
| I4-P2 | Positive | Positive | Positive | Positive |
| I4-P4 | Negative | Negative | Negative | Negative |
| I5-P3 | Positive | Positive | Positive | Positive |
| I5-P4 | Negative | Negative | Negative | Negative |
| precision | | 1.00 | 0.75 | 1.00 |
| recall | | 1.00 | 0.75 | 0.80 |
| F1 | | 1.00 | 0.75 | 0.89 |

Figure 11 shows the interwell connectivity analysis results of well I1 using NCC. Compared with the results of the proposed method (Figure 8), NCC has two limitations:

1. For the injection–production pair I1-P1 with a proven high-permeability streak, the connectivity calculated by NCC (0.84) is lower than that of the proposed method (0.9);
2. For injection–production pairs connected by non-preferential flow paths, the connectivity calculated by NCC (P2: 0.81, P3: 0.69, P4: 0.44) is higher than that of the proposed method (P2: 0.72, P3: 0.66, P4: 0.38), which directly leads to the misclassification of injection–production pair I1-P2 as strongly connected.

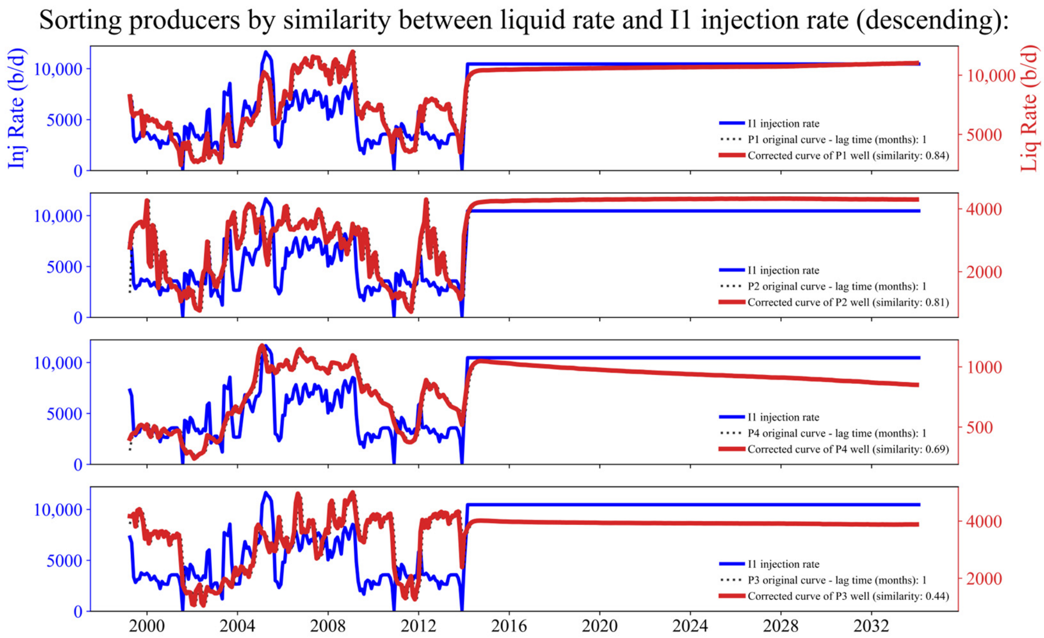


**Figure 11.** Connectivity analysis for well I1 by NCC. Note: red line—original liquid production curve shifted forward by lag time.

Further analysis reveals three core reasons for these limitations:

1. NCC calculates similarity based on the full length of the curve. For injection–production pair I1-P1, non-key regions reduce the overall similarity, while for other injection–production pairs, non-key regions inflate the overall similarity.

2. The time lag calculation of NCC relies on shifting the entire production curve to find the time difference corresponding to the maximum similarity. This full-curve matching constrains the time lag to a fixed value throughout the entire production period, which may fail to capture visually similar fluctuations.
3. The NCC algorithm only focuses on the synchronization of fluctuations when evaluating similarity, with the magnitude of the fluctuation slope having almost no impact on the results. This may lead to high similarity scores between large injection fluctuations and minor daily production fluctuations, making the results more susceptible to noise interference.

Figure 12 shows the fitting performance of CRM for the liquid production rate of the four producers. Despite the excellent history matching performance, CRM still presents misclassification, which is most likely caused by the non-uniqueness of inversion fitting.

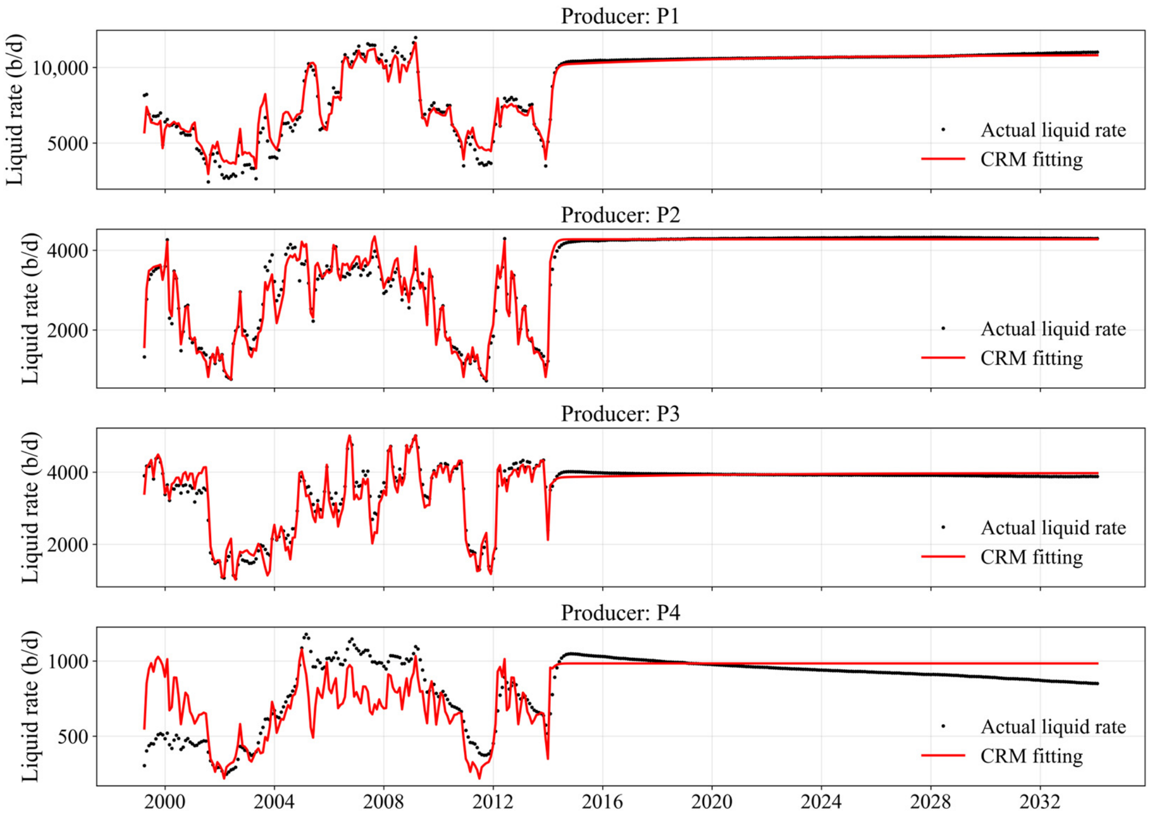


**Figure 12.** CRM history matching results for producers.

This reflects the reliability limitation of such methods in field applications: engineers cannot judge the reliability of the analysis results solely from the outputs of CRM or machine learning-based methods, and must rely on comprehensive understanding from injection–production response analysis, monitoring data interpretation and other independent sources. Without supporting evidence from additional analyses, the outputs of these methods can only be either fully accepted or completely rejected. In contrast, the proposed method is developed based on the fundamental principle of injection–production response analysis and is essentially an automated implementation of systematic injection–production response analysis. Its output results (Figure 8) explicitly mark the matched target regions and the corresponding injection–production curves, enabling engineers to quickly identify potential misclassifications even without additional supporting data. This significantly reduces the manual workload of injection–production response analysis and delivers higher reliability compared with other benchmark methods.

https://doi.org/10.3390/en19184285

3.3.2. Real Field-Case Comparison

In the real field case, the comprehensive multi-data understanding of the reservoir was taken as the ground truth for F1-score calculation, where I1-P1 and I1-P6 were defined as strongly connected injection–production pairs (positive cases), and the rest as weakly connected injection–production pairs (negative cases). The results of the proposed method, NCC and CRM, were taken as the predicted values and substituted into Equations (5)–(7) to calculate the matching performance against the ground truth, so as to verify the field applicability of the proposed method. The F1-score results are summarized in Table 2.

**Table 2.** F1-score results for actual well groups.

| Injector–Producer Pair | Actual | The Proposed Method | NCC | CRM |
|---|---|---|---|---|
| I1-P1 | Positive | Positive | Negative | Positive |
| I1-P2 | Negative | Negative | Negative | Positive |
| I1-P3 | Negative | Negative | Negative | Positive |
| I1-P4 | Negative | Negative | Negative | Positive |
| I1-P5 | Negative | Negative | Positive | Positive |
| I1-P6 | Positive | Positive | Positive | Positive |
| I1-P7 | Negative | Negative | Negative | Positive |
| I1-P8 | Negative | Negative | Negative | Positive |
| precision | | 1.00 | 0.50 | 1.00 |
| recall | | 1.00 | 0.50 | 0.25 |
| F1 | | 1.00 | 0.50 | 0.40 |

Table 2 shows that the proposed method achieves an F1-score of 1 in the real field case, indicating excellent field application performance. CRM delivers poor performance with an F1-score of 0.4, as it identifies all injection–production pairs as strongly connected and requires extremely time-consuming history matching. NCC outperforms CRM but is inferior to the proposed method, with an F1-score of 0.5.

These results highlight the challenge of history matching for physics-based inversion methods such as CRM in real field applications. In contrast, signal processing-based methods including the proposed method and NCC deliver more accurate results with significantly lower computational cost. Specifically, signal processing methods perform independent analysis for each well group, meaning that the number of well groups does not affect the analysis accuracy, the computation time increases linearly with the number of well groups, and no time-consuming history matching process is required.

To evaluate the robustness of the empirical parameters, sensitivity analyses were performed by varying the weighting coefficient $\alpha$ from 0.6 to 0.8, the similarity filtering threshold from 0.4 to 0.6, and the segmentation-window extension limits (lower bound from 2 to 4 months, upper bound from 8 to 10 months). The overall connectivity classification remained largely stable, with only minor variations among moderate-connectivity pairs and no significant impact on the final connectivity results. Furthermore, the same parameter set was used for both the synthetic and field cases without modification, and accurate results were obtained in both cases under distinct geological conditions, further confirming the reliability of the selected parameters.

## 4. Discussion

This study proposes a novel method for interwell connectivity identification based on the similarity of injection and production rate fluctuations. While early studies have adopted curve similarity analysis for connectivity characterization, these methods are universally built on the overall amplitude of the full curve, rather than the slope of the curve in key fluctuation regions. This full-curve amplitude-based approach has three critical limitations that compromise the accuracy of identification results:

1. Similarity in the overall amplitude of injection and production curves is not equivalent to similarity in the magnitude of rise and fall of fluctuations, meaning a high overall similarity score cannot reliably indicate a strong injection–production response relationship;
2. Full-curve holistic matching cannot mitigate the interference of noise from non-key regions on the final similarity results;
3. Full-curve matching is based on the assumption of a constant time lag, which leads to misclassification of low similarity due to minor curve misalignment in real field scenarios with time-varying time lag, and may result in truly strongly connected injection–production pairs being incorrectly identified as low-correlation pairs.

The novel method proposed in this study quantifies the similarity of injection–production rate fluctuations with the curve slope as the core calculation object. The workflow consists of screening regions with significant fluctuations, performing segmented matching of fluctuation similarity, outlier filtering, and weighted fusion to obtain the final comprehensive similarity for each injection–production pair. The results demonstrate that the similarity calculated by the proposed method has a higher consistency with the actual interwell connectivity. Compared with the widely used CC method [31] and CRM method [7], the proposed method delivers superior performance in both the synthetic heterogeneous reservoir model and the real field well group case.

It is worth noting that the proposed method has several inherent limitations:

1. It may deliver degraded performance for wells with a short water flooding duration or stable injection rates with no significant fluctuations.
2. In terms of applicability, the proposed method is theoretically suitable for all reservoirs conforming to the injection–production response law, but this study only validates its applicability in water flooding scenarios of porous carbonate reservoirs in the Middle East. Its adaptability to other reservoir types and gas flooding development remains to be further verified.
3. The current version of the method only uses injection and production dynamic data, which introduces a certain degree of uncertainty. Specifically, there may be spurious correlations where highly similar fluctuations are observed between injection–production pairs with no actual physical connectivity. Subsequent studies will integrate additional data sources or auxiliary methods to further improve the identification accuracy.
4. The outlier filtering step of the proposed method is built on the assumption that the time lag does not exhibit a sustained increasing trend over time; therefore, scenarios with continuously rising time lag are not accounted for in the method design, and the proposed method is not applicable to such cases.

We also conducted full-field interwell connectivity analysis for more than 500 wells in the target oilfield. The preliminary results show that the directions of strong interwell connectivity identified by the proposed method have a high correlation with the location of high-permeability streaks in the detailed geological model, although this finding is still preliminary and requires further in-depth validation. For future research, we plan to extend the proposed method to multi-layer reservoir scenarios by integrating perforation data and production monitoring data. We will also explore the combination of the proposed method with intelligent decision-making systems to conduct research on intelligent optimization of injection and production rate allocation based on the interwell connectivity results.

## 5. Conclusions

1. To address the low accuracy of interwell connectivity identification caused by direct application of general-purpose signal processing algorithms in existing studies, this paper proposes a novel injection–production response-based method for interwell connectivity characterization. Taking curve slope as the core calculation object and considering time-varying time lag, the method improves identification accuracy via segmented matching of key fluctuation regions, outlier filtering and multi-weighted fusion, and can also assist in roughly estimating the formation timing of preferential flow paths.
2. Validation results from both synthetic heterogeneous and real field carbonate reservoir cases show that the proposed method achieves better consistency with actual interwell connectivity than conventional NCC and CRM methods. It is insensitive to null values in field data, and its output results are easy to verify, with low uncertainty and high reliability.
3. The method has limitations: It may deliver degraded performance for wells with short water flooding duration or no significant injection rate fluctuations, and it does not cover scenarios with continuously increasing time lag.

**Author Contributions:** Conceptualization, H.S. and C.Y.; methodology, H.S.; software, H.S.; validation, Z.X. and J.L.; formal analysis, Y.L.; investigation, H.S. and H.H.; resources, Z.X.; data curation, C.Y.; writing—original draft preparation, H.S.; writing—review and editing, H.S., C.Y. and Y.L.; visualization, H.S. and H.Y.; supervision, C.Y.; project administration, Z.X.; funding acquisition, C.Y. All authors have read and agreed to the published version of the manuscript.

**Funding:** This research was funded by the Major Science and Technology Special Project of the China National Petroleum Corporation, "Research on Key Technologies for Efficient Production of Overseas Large-scale Carbonate Reservoirs" (Grant No. 2023ZZ19-07).

**Data Availability Statement:** Data are unavailable due to privacy restrictions.

**Conflicts of Interest:** Authors Hao Sun, Chao Yang, Zhaohui Xia, Yuedong Lu, and Jianbo Liu were employed by the Research Institute of Petroleum Exploration and Development, PetroChina. Authors Huajun Hu and Heng Yang were employed by the China National Oil and Gas Exploration and Development Company LTD. The authors declare that this study received funding from the Major Science and Technology Special Project of the China National Petroleum Corporation. The funder was not involved in the study design, collection, analysis, interpretation of data, the writing of this article or the decision to submit it for publication.

## Abbreviations

The following abbreviations are used in this manuscript:

| | |
|---|---|
| $A$ | vector A |
| $B$ | vector B |
| CC | Cross-Correlation |
| CRM | Capacitance-Resistance Model |
| $\cos\theta$ | cosine similarity |
| $\Delta t$ | time lag |
| $F_1$ | the weighted harmonic mean of precision and recall |
| $FN$ | incorrectly predicted negative cases |
| $FP$ | incorrectly predicted positive cases |
| $\lambda$ | the amplitude weight |
| $n$ | the total number of paired data points |

| | |
|---|---|
| NCC | Normalized Cross-Correlation |
| *precision* | the proportion of predicted preferential flow directions that are actual preferential flow directions |
| *recall* | the proportion of correctly identified actual preferential flow directions out of all real preferential flow directions |
| RMSE | Root Mean Square Error |
| $s$ | the similarity calculated by the proposed method |
| $TN$ | correctly predicted negative cases |
| $TP$ | correctly predicted positive cases |
| $x_{pro}$ | the position index of the production segment center point |
| $y_{inj,i}$ | the i-th slope data point of the injection curve |
| $y_{pro,i}$ | the i-th slope data point of the production curve |
| $y_{inj}$ | the curve value in the injection target segment |
| $y_{pro}$ | the curve value in the matched production segment |

## References

1. Zhang, Y.; Jiang, R.; Zheng, X. Inter-Well Tracer Analysis Technology. *J. Univ. Pet. (Nat. Sci. Ed.)* **2001**, *25*, 76–78.
2. Du, W.; Zhang, J.; Hao, S. Application of Pulse Well Testing in the Pilot Test Well Group of Tertiary Oil Recovery in Yumen. *Oil Gas Well Test.* **2002**, *4*, 32–33+76.
3. Wen, Z.; Zhu, D.; Li, Y.; Zhang, G. Application of Chromatographic Fingerprint Technology to Study the Connectivity of Oil Reservoirs in Block 6 of Gudong Oilfield. *Pet. Explor. Dev.* **2004**, *1*, 82–83.
4. Sun, L.; Li, B.; Liu, F. Efficient Management of Water Flooding Reservoirs Based on Pollock Streamline Tracing. *Lithol. Reserv.* **2021**, *33*, 169–176.
5. Setiyawan, H.; Evelyn, K.; Hisan, R.F.; Fardiansyah, I. Subsurface Waterflood Management Improvement: The Art of Reservoir Connectivity Characterization. In *Proceedings of the SPE Improved Oil Recovery Conference*; SPE: Tulsa, OK, USA, 2024; p. D021S010R003.
6. Zhao, H.; Kang, Z.; Sun, H.; Zhang, X.; Li, Y. An Interwell Connectivity Inversion Model for Waterflooded Multilayer Reservoirs. *Pet. Explor. Dev.* **2016**, *43*, 99–106. [CrossRef]
7. Yousef, A.A.; Gentil, P.H.; Jensen, J.L.; Lake, L.W. A Capacitance Model to Infer Interwell Connectivity from Production and Injection Rate Fluctuations. *SPE Reserv. Eval. Eng.* **2006**, *9*, 630–646. [CrossRef]
8. Albertoni, A.; Lake, L.W. Inferring Interwell Connectivity Only From Well-Rate Fluctuations in Waterfloods. *SPE Reserv. Eval. Eng.* **2003**, *6*, 6–16. [CrossRef]
9. Liang, X. A Simple Model to Infer Interwell Connectivity Only from Well-Rate Fluctuations in Waterfloods. *J. Pet. Sci. Eng.* **2010**, *70*, 35–43. [CrossRef]
10. Sayarpour, M.; Zuluaga, E.; Kabir, C.S.; Lake, L.W. The Use of Capacitance-Resistive Models for Rapid Estimation of Waterflood Performance and Optimization. In *Proceedings of the SPE Annual Technical Conference and Exhibition*; SPE: Anaheim, CA, USA, 2007; p. SPE-110081-MS.
11. Moreno, G.A.; Lake, L.W. Input Signal Design to Estimate Interwell Connectivities in Mature Fields from the Capacitance-Resistance Model. *Pet. Sci.* **2014**, *11*, 563–568. [CrossRef]
12. Zhang, Z.; Li, H.; Zhang, D. Water Flooding Performance Prediction by Multi-Layer Capacitance-Resistive Models Combined with the Ensemble Kalman Filter. *J. Pet. Sci. Eng.* **2015**, *127*, 1–19. [CrossRef]
13. Davudov, D.; Agarwal, A.; Varma, A.; Venkatraman, A.; Osei, K. A Data-Driven Approach to Optimize WAG Injection in a Large Carbonate Field. In *Proceedings of the SPE Improved Oil Recovery Conference*; SPE: Tulsa, OK, USA, 2024; p. D021S006R005.
14. Zhao, H.; Li, Y.; Gao, D.; Cao, L. Research on Reservoir Interwell Dynamic Connectivity Using Systematic Analysis Method. *Acta Pet. Sin.* **2010**, *31*, 633–636.
15. Li, Y.; Zhang, L.; Chen, Y.; Hu, D.; Ma, R.; Wang, S.; Li, Q.; Liu, D. An Intelligent Integrated Production Optimization Technique for Waterflooding Reservoirs. *Pet. Explor. Dev.* **2025**, *52*, 677–691. [CrossRef]
16. Liu, W.; Liu, W.D.; Gu, J. Reservoir Inter-Well Connectivity Analysis Based on a Data Driven Method. In *Proceedings of the Abu Dhabi International Petroleum Exhibition & Conference*; SPE: Abu Dhabi, United Arab Emirates, 2019; p. D022S178R001.
17. Zeng, X.; Zhang, W.; Chen, T.; Jacobsen, H.-A.; Zhou, J.; Chen, B. Evaluating Interwell Connectivity in Waterflooding Reservoirs with Graph-Based Cooperation-Mission Neural Networks. *SPE J.* **2022**, *27*, 2443–2452. [CrossRef]
18. Saihood, T.; Saihood, A.; Al-Shaher, M.A.; Ehlig-Economides, C.; Zargar, Z. Fast Evaluation of Reservoir Connectivity via a New Deep Learning Approach: Attention-Based Graph Neural Network for Fusion Model. In *Proceedings of the SPE Annual Technical Conference and Exhibition*; SPE: New Orleans, LA, USA, 2024; p. D011S010R006.

19. Zhao, Y.; Li, H.; Zeng, X.; Ge, F.; Zhang, L.; Wang, L.; Liao, B.; Xiao, Q. Research on Inter-Well Connectivity of Water-Flooding Reservoir: Temporal Neural Network Based on Graph Structure. *Geoenergy Sci. Eng.* **2024**, *242*, 213221. [CrossRef]
20. Huang, Z.-Q.; Wang, Z.-X.; Hu, H.-F.; Zhang, S.-M.; Liang, Y.-X.; Guo, Q.; Yao, J. Dynamic Interwell Connectivity Analysis of Multi-Layer Waterflooding Reservoirs Based on an Improved Graph Neural Network. *Pet. Sci.* **2024**, *21*, 1062–1080. [CrossRef]
21. Tian, C.; Horne, R.N. Inferring Interwell Connectivity Using Production Data. In *Proceedings of the SPE Annual Technical Conference and Exhibition*; SPE: Dubai, United Arab Emirates, 2016; p. D031S051R004.
22. Hernandez-Mejia, J.L.; Pisel, J.; Jo, H.; Pyrcz, M.J. Dynamic Time Warping for Well Injection and Production History Connectivity Characterization. *Comput. Geosci.* **2023**, *27*, 159–178. [CrossRef]
23. Wang, Y.; Kabir, C.S.; Reza, Z. Deciphering Well Connectivity with Diagnostic Signal Processing Techniques. *J. Pet. Sci. Eng.* **2020**, *185*, 106610. [CrossRef]
24. Unal, E.; Siddiqui, F.; Rezaei, A.; Eltaleb, I.; Kabir, S.; Soliman, M.Y.; Dindoruk, B. Use of Wavelet Transform and Signal Processing Techniques for Inferring Interwell Connectivity in Waterflooding Operations. In *Proceedings of the SPE Annual Technical Conference and Exhibition*; SPE: Calgary, AB, Canada, 2019; p. D031S056R002.
25. Jansen, J.-D.; van den Hoek, P.J.; Zwarts, P.J.; Al-Masfry, R.; Hustedt, B.; van Schijndel, L. Behaviour and Impact of Dynamic Induced Fractures in Waterflooding and EOR. In *The 42nd U.S. Rock Mechanics Symposium (USRMS)*; U.S. Rock Mechanics/Geomechanics Symposium: Tucson, AZ, USA, 2008.
26. Li, Y.; Sun, Z.; Ma, K.; Jiang, R.; Hua, J. Numerical Simulation Study on Deep Profile Control and Flooding Technology Considering Time-Varying Permeability. *J. Chongqing Univ. Sci. Technol. (Nat. Sci. Ed.)* **2019**, *21*, 71–76. [CrossRef]
27. Wang, Y.; Song, X.; Tian, C.; Shi, C.; Li, J.; Hui, G.; Hou, J.; Gao, C.; Wang, X.; Liu, P. Dynamic Fractures Are an Emerging New Development Geological Attribute in Water-Flooding Development of Ultra-Low Permeability Reservoirs. *Pet. Explor. Dev.* **2015**, *42*, 222–228. [CrossRef]
28. Wang, J.; Song, X.; Fu, Y.; Sun, L.; Xu, J. Time-Varying Permeability of Sandstone Reservoirs under Waterflooding of Different Water Quality. *Oil Gas Geol.* **2021**, *42*, 1234–1242.
29. Xu, J.; Guo, C.; Wei, M.; Jiang, R. Impact of Parameters' Time Variation on Waterflooding Reservoir Performance. *J. Pet. Sci. Eng.* **2015**, *126*, 181–189. [CrossRef]
30. Virtanen, P.; Gommers, R.; Oliphant, T.E.; Haberland, M.; Reddy, T.; Cournapeau, D.; Burovski, E.; Peterson, P.; Weckesser, W.; Bright, J.; et al. SciPy 1.0: Fundamental Algorithms for Scientific Computing in Python. *Nat. Methods* **2020**, *17*, 261–272. [CrossRef] [PubMed]
31. Wang, Y.; Kabir, C.S.; Reza, Z. Inferring Well Connectivity in Waterfloods Using Novel Signal Processing Techniques. In *Proceedings of the SPE Annual Technical Conference and Exhibition*; SPE: Dallas, TX, USA, 2018; p. D021S016R004.